SURFACE AND INTERFACE ANALYSIS
Surf. Interface Anal. **27**, 618–628 (1999)

Application of Parallel Factor Analysis and X-ray Photoelectron Spectroscopy to the Initial Stages in Oxidation of Aluminium I. The Al 2p Photoelectron Line

T. Do,*[,1] N. S. McIntyre,[2] R. A. Harshman,[3] M. E. Lundy[3] and S. J. Splinter[4]

[1] Department of Materials & Mechanical Engineering, and Surface Science Western, University of Western Ontario, London, Ontario, Canada N6A 5B9

[2] Surface Science Western and Department of Chemistry, University of Western Ontario, London, Ontario, Canada N6A 5B7

[3] Department of Psychology, University of Western Ontario, London, Ontario, Canada N6A 5C2

[4] BC Research Inc., British Columbia, Canada V6S 2L2

Three-way parallel factor analysis (PARAFAC) has been used to decompose a set of x-ray photoelectron spectroscopy (XPS) spectra that result during the oxidation of aluminium surfaces. The Al 2p core-level photoelectron lines have been used to follow oxide film growth on clean aluminium surfaces as a function of exposure time and pressure of water vapour. In this paper, a fine peak structure of the XPS Al 2p spectrum has been extracted using PARAFAC. The PARAFAC solution provides new information on elemental processes in the very initial stages of oxidation kinetics, showing new components in the XPS spectrum as well as their evolution through a range of time and pressure variables. As expected, the reaction of water vapour with aluminium results in attenuation of the metallic peak at binding energy (BE) 72.87 ± 0.05 eV and an increase of the oxidic peak at BE 75.80 ± 0.05 eV. However, an additional factor is also identified, which suggests the formation of an interfacial metal hydride at BE 72.4(4) eV, as well as a concomitant oxide peak at 75.4(3) eV. Both are ascribed to products of the hydrolysis of adsorbed water molecules at the aluminium interface. At pressures above and below 1.3×10^{-5} Pa this factor is diminished; in the case of higher pressure, this is ascribed to an increase of the recombination of atomic hydrogen.

KEYWORDS: aluminium oxide; aluminium hydride; oxidation; parallel factor analysis; XPS

INTRODUCTION

X-ray photoelectron spectroscopy (XPS) is a primary tool in the quantitative analysis of solid surfaces, especially for the detection of changes in the chemical state of near-surface atoms. A number of applications have established its great importance in chemistry, from both basic science and technological viewpoints. In general, the formalism of quantitative XPS involves two distinguishable procedures: the identification of recorded signals or peaks in a spectrum; and measurement of the photoelectron intensity.[1] The first process is the crucial and most difficult step in the effort to obtain good quantitative results; the successful analysis requires one to be able to identify signals due to all constituents or electron-scattering processes present in the analysed area. In the second step, although most calculations are fairly straightforward, the final results can be reliable only if the relation between the intensity of the measured signal and the concentration is definable. In practice, there is no problem in quantitative analysis using XPS for well-defined systems, i.e. a traditional curve-fitting technique can be used to identify all signals. However, in more complicated cases, where several peaks representing different chemical environments of an element closely overlap or where more than one variable changes simultaneously, the curve-fitting technique cannot provide an answer without some measure of uncertainty. In analysis an unknown XPS spectrum, without prior references from the literature, there are always two open questions concerning the ambiguity of the solution: how many peaks are present and what are their positions in binding energy?

Figure 1 shows an example of two different solutions of decomposition for the same XPS Al 2p photoelectron line using a curve-fitting technique performed with the same level of goodness of fit (χ^2 value). While the two main peaks representing Al^0 (metallic) and Al^{3+} (oxidic) states can be distinguished clearly, there is at least one other possible peak between them that can be assigned to one or more additional chemical states.[2–4] The metallic peak can be split also into two parts, corresponding to the $2p_{1/2}$ and $2p_{3/2}$ lines. Most earlier studies has used only these two main peaks to interpret results.

For analysis of a series of XPS spectra measured as a function of one physical variable, e.g. concentration or pressure, which sets a two-dimensional data matrix, a

* Correspondence to: T. Do, Surface Science Western, University of Western Ontario, London, Ontario, Canada N64 5B7. E-mail: thando@surf.ssw.uwo.ca.

CCC 0142–2421/99/070618–11 $17.50

Received 14 July 1998
Revised 10 December 1998; Accepted 14 December 1998

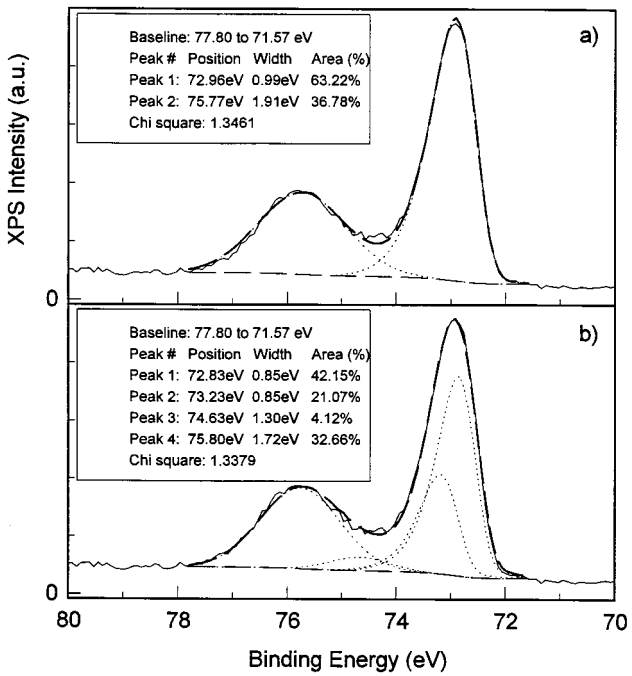

Figure 1. Decomposition of the XPS Al 2p spectrum using the curve-fitting technique with: (a) two peaks; (b) four peaks. Calculations were performed using software developed by Surface Science Laboratories, Inc.

statistical technique called principal component analysis (PCA) or factor analysis (FA) has been employed with varying degrees of success.[5–7] The use of PCA is often limited by the difficulty in finding a correct rotation (or transformation) for the final solution. However, the above techniques are unable to deal with a three-dimensional data matrix, i.e. the case where two physical variables simultaneously influence the XPS spectrum. In the present work, the oxidation of aluminium surfaces has been investigated using the XPS technique. Several series of XPS Al 2p spectra measured as a function of oxidation time *and* pressure of water vapour were used to create a three-dimensional XPS data matrix. The XPS data have been analysed using the parallel factor analysis (PARAFAC) method. The decomposition of XPS spectra in PARAFAC is based on the variation of peak components through both oxidation time and pressure parameters; this results in a much higher degree of confidence of the analysis compared with the one-variable analysis. From this analysis three component peaks have been identified in the XPS Al 2p spectrum that are influenced by oxidation time and pressure variables.

PRINCIPLES OF PARALLEL FACTOR ANALYSIS

Parallel factor analysis is a three-way decomposition method developed as an improvement to the traditional two-way factor analysis method. Founded independently by Harshman[8] and by Carroll and Chang[9] and used initially in psychometrics, the PARAFAC method has recently attracted more interest from other areas of science, particularly in chemometrics,[10–12] including an independent rediscovery.[13]

The n-factor PARAFAC model is expressed mathematically as[8]

$$y_{ijk} = \sum_{f=1}^{n} a_{if} b_{jf} c_{kf} + e_{ijk} \quad (1)$$

where the quantity y_{ijk} measured at level i of variable A, level j of B and level k of C is a linear combination of n factors; each is determined by three factor loadings or a_{if}, b_{jf} and c_{kf} for the ith level of variable A, the jth level of B and the kth level of C, respectively; e_{ijk} is the residual or error term. If we assume that three independent variables A, B and C will affect a quantity y and that one measures the effect for all combinations of r levels of A, c levels of B and s levels of C, then the data can be assembled into a three-way array $\boldsymbol{Y}$ of dimension $r \times c \times s$. The variables A, B and C can be viewed as the three 'ways' of measurement in $\boldsymbol{Y}$, i.e. rows, columns and slices, and are often referred to respectively, as 'Mode A', 'Mode B' and 'Mode C'; the factor loadings a_{if}, b_{jf} and c_{kf} are elements of matrices $\boldsymbol{A}$, $\boldsymbol{B}$ and $\boldsymbol{C}$. It should be noted that the model does not fit interaction between factors; for example, there is no term for factor 1 in $\boldsymbol{A}$ combined with factor 2 in $\boldsymbol{B}$ and $\boldsymbol{C}$. The essence of the PARAFAC method lies in the fact that the pure factor loadings extracted in a mode represent the factor variation for only one variable unaffected by the others. This means that a complex multi-variable set of data can be split into one-variable sets that are readily interpretable systems using three-way PARAFAC analysis.

Estimation of the PARAFAC model requires a best fit of the model to the data, i.e. minimization of the function

$$Q = \sum_{i=1}^{r} \sum_{j=1}^{c} \sum_{k=1}^{s} e_{ijk}^2 \quad (2)$$

followed by standardization of column mean squares in two of the three matrices $\boldsymbol{A}$, $\boldsymbol{B}$ and $\boldsymbol{C}$ and compensatory adjustment of column mean squares in the third matrix. This minimization is often accomplished by means of an alternating least-squares (ALS) estimation procedure. The ALS algorithm repeatedly solves three linear regression problems. In the computational routine, after the number of factors n is selected, the calculations will take the following steps:

(1) Step 1: initialize the factor loadings in modes $\boldsymbol{B}$ and $\boldsymbol{C}$ by random or eigen structure.
(2) Step 2: estimate the factor loadings in mode $\boldsymbol{A}$ from $\boldsymbol{B}$ and $\boldsymbol{C}$ and the data $\boldsymbol{Y}$ by least-squares regression.
(3) Step 3: estimate mode $\boldsymbol{B}$ likewise, using $\boldsymbol{A}$, $\boldsymbol{C}$ and $\boldsymbol{Y}$.
(4) Step 4: estimate mode $\boldsymbol{C}$ likewise, using $\boldsymbol{A}$, $\boldsymbol{B}$ and $\boldsymbol{Y}$.
(5) Step 5: repeat steps 2–4 until the convergence criterion is reached (usually a minimum difference in fit or factor loadings between estimations is used).

The above process is repeated using several different random starts in step 1 to confirm that convergence is at a global minimum for Eqn. (2). The main advantage of the PARAFAC method is the singularity of its solution, which can be proved mathematically.[12,14–18] Unlike factor analysis, there is no rotation or transformation problem in the PARAFAC technique.

A physically interpretable solution requires that the factor loadings must be non-negative in all modes. In theory, if all factors have adequately independent variation in all three modes, the singular property of the

PARAFAC model will be enough to ensure non-negativity of the recovered loadings. However, because of noise in the data and because factors may not always show the required distinct variation in all modes, it is highly desirable to incorporate a non-negativity constraint on the recovered parameters. If an ALS algorithm is being used for estimation, this constraint can be incorporated by means of non-negative least-squares regression.[19] This has been successfully applied to spectroscopic data.[20]

In the case where the expected standard deviation of the measurement error changes from element to element in the data matrix, the weighted least-squares algorithm[21] offers a better fitted solution. The weighted minimizing function from Eqn. (2) is now defined as

$$Q_w = \sum_{i=1}^{r}\sum_{j=1}^{c}\sum_{k=1}^{s} w_{ijk}\, e_{ijk}^2 \tag{3}$$

where w_{ijk} is the weight given to y_{ijk}. Usually, in order to ensure the solution with minimum variance, the weights must be equal or close to $1/s_{ijk}^2$, where s_{ijk} is the estimated standard deviation of y_{ijk}. This requires that the standard deviation of each element in the data matrix has to be known or it has to be estimated prior to the analysis.

PARALLEL FACTOR ANALYSIS PROGRAMS

There are three programs for three-way analysis available, two of which are in the public domain. A PARAFAC program written in Fortran by Margaret E. Lundy and Richard A. Harshman from the University of Western Ontario, London, Ontario, Canada, with an option for an orthogonality constraint, is mainly used in psychology and social sciences and is available at: http://www.uwo.ca/its/ftp/pub/misc/parafac/ or at ftp://ftp.uwo.ca/pub/misc/parafac/. More details about the method and algorithm can be found in a review paper.[17] Another algorithm coded in the MATLAB language, offered by Rasmus Bro, Royal Veterinary and Agricultural University, Denmark, contains useful options for constraint on orthogonality and non-negativity. This program is available at: http://newton.mli.kvl.dk/Matlab/PARAFAC_Bro/. A third program 'PMF3' (three-way positive matrix factorization[22]) in written is Fortran by Pentti Paatero, University of Helsinki, Finland, and is based on a curve-fitting type of optimization method instead of an ALS algorithm. It allows one to incorporate both a weighted least-squares regression and a non-negativity constraint. This program was applied, along with its two-way analogue, to environmental data in a paper by Paatero and Tapper.[23] In this paper the 'PMF3' program was used to analyse the XPS data. The weighted regression and the non-negativity constraints implemented in the 'PMF3' program seem to be essential for analysing the XPS data, which consisted of spectra collected with different experimental parameters and characterized by different standard deviations. In fact, the results presented later show that, without the non-negativity constraint, solutions are obtained with negative factor loadings that have no physical interpretation; also, the unweighted regression cannot provide a satisfactory fit, and solutions were characterized by high χ^2 values. However, with these features in place, the 'PMF3' program has been a very successful tool in three-way analysis of spectral data.

X-RAY PHOTOELECTRON SPECTRA IN THREE-WAY MODEL

In general, the XPS intensity measured by the photoelectron current in an XPS experiment can be written in the form[24]

$$I_Z(E) = \Phi(h\nu)\sigma_Z(h\nu)N_Z\,\lambda(E)\cos(\psi)F(E)T(E)D(E) \tag{4}$$

where $I_z(E)$ is the measured current of photoelectrons of kinetic energy E from an element Z, $\Phi(h\nu)$ is the x-ray flux on the sample at the characteristic energy $h\nu$, $\sigma_z(h\nu)$ is the cross-section for photoelectron production of element Z, N_z is the atomic density of element Z, $\lambda(E)$ is the inelastic mean free path of photoelectrons of kinetic energy E, ψ is the angle between the photoelectron direction and the normal to the sample surface, $F(E)$ is an electron-optical factor, $T(E)$ is the analyser transmission function and $D(E)$ is the efficiency of the electron detector.

Equation (4) represents a simplified model based on a proportional relationship between the measured signal intensity and the concentration. This model assumes also the exclusivity of various processes occurring in photoelectron emission phenomena and instruments related during its measurements. It can be further generalized and expressed in the form

$$I_Z(E) = CI_1(E)\ldots I_i(E)\ldots I_n(E)N_Z \tag{5}$$

where C is a proportional parameter, independent from concentration and $I_i(E)$ is a concentration-dependent correction factor for the ith physical effect, e.g. elastic collision, backscattering effect, etc. An XPS spectrum of an element is usually a sum of several peaks representing its chemical shifts due to different bonding environments in the analysed area; the spectral intensity then can be expressed as a sum of contributions from all peak components

$$I_{Z,ij}(E) = \sum_{f=1}^{n} I_{Z,ijf}(E) + e_{ij}(E) \tag{6}$$

or in a fully developed form

$$I_{Z,ij}(E) = \sum_{f=1}^{n} I_{Z,f}(E)a_{if}\,b_{jf} + e_{ij}(E) \tag{7}$$

where n here is the number of peaks present in a given XPS spectrum; indexes i and j indicate the ith and jth levels of two other physical parameters a and b, respectively, e.g. concentration and pressure, which simultaneously affect the XPS intensity; and $e_{ij}(E)$ is the error term. It should be noted that a level here is an ordered number represented by a certain value of a physical variable. By defining the number of peaks as the factor number, the similarity of Eqn. (7) to the trilinear model described by Eqn. (1) ensures the applicability of the PARAFAC technique to analysis of the XPS data. However, our motivation to apply the PARAFAC technique is to make use of its specificity to determine the factor number and its variations, i.e. its main advantage

over other methods, particularly the curve-fitting technique. Only the PARAFAC technique can deal with a case where the co-varying contributions from two independent sources can produce a multi-peak factor. The factor loadings extracted by PARAFAC represent the factor variation as a function of *only* one variable, *without any interaction from the others*. Assuming no ambiguity in number of peaks or peak positions, the curve-fitting technique can only provide a solution determined by Eqn. (6). However, each peak found by curve fitting represents contributions from all physical effects; there is no way that one can obtain the variation of individual peaks as a function of a single variable. By contrast, PARAFAC is able to obtain the number of peaks and peaks positions as well as their variations [see Eqn. (7)].

The above model of three-way XPS data Eqn. (7) has been tested extensively using the 'PMF3' program on simulated data. The goal of these tests was to examine the applicability and limitations of the three-way method in analysing XPS data as well as to determine the data treatment that might need consideration prior to applying the three-way analysis. Several sets of XPS Al 2p synthetic spectra were created using simple Gaussian peaks that simulated the oxidation process on an aluminium surface as a function of exposure time and water vapour pressure. To these Gaussian peaks the following real spectral features from the XPS Al 2p photoelectron lines are added: differences in peak width, mixed Lorentzian and Gaussian character, peak asymmetry due to plasmon excitation, background effects of inelastic scattering and various types of random errors. Two important properties have been established:

(1) The three-way solutions are unreliable if any kind of background is included, therefore real XPS spectra should have background and baselines removed prior to three-way analysis.
(2) The three-way technique is sensitive to the number of factors used (=number of peaks) in analysing the XPS data. An incorrect number of peaks leads to deformed peak shapes and degenerate solutions. These kinds of results were also obtained if two or more factors were simulated that were closely similar in their variation in one or two modes.

EXPERIMENTAL

Polycrystalline aluminium (99.999% purity) was supplied by Alcan Aluminum Ltd., Kingston, Ontario. Crystallographic orientation of the large grain faces ($\sim$100 μm diameter) was determined using an electron backscattering diffraction technique, which showed low-index orientations on all grains. Specimens were polished to a 0.05 μm Al_2O_3 finish, degreased ultrasonically, annealed in a vacuum (573 K, 30 min) and cleaned by Ar^+ ion bombardment (3 keV, 10 min). Clean surfaces were then exposed to water vapour in a separate custom-designed preparation chamber attached to the XPS spectrometer at pressures ranging from 2.0×10^{-6} to 6.5×10^{-4} Pa through six levels ($p(1) = 2.0 \times 10^{-6}$, $p(2) = 7.8 \times 10^{-6}$, $p(3) = 1.3 \times 10^{-5}$, $p(4) = 6.5 \times 10^{-5}$, $p(5) = 1.3 \times 10^{-4}$ and $p(6) = 6.5 \times 10^{-4}$ Pa) and exposure times from 1 to 60 min at 15 separate time levels for every minute up to 10 min and after that for 15, 20, 30, 45 and 60 min. After exposure to water vapour the sample was transferred back into the XPS analytical chamber and an XPS spectrum was measured at an operating base pressure of 4.0×10^{-7} Pa. All XPS spectra were obtained using a Surface Science Laboratories SSX-100 spectrometer equipped with a monochromatic Al Kα (1486.6 eV) x-ray source; the binding energy scale (i.e. kinetic energy scale) was calibrated to give an Au $4f_{7/2}$ photoelectron line position at 83.98 eV. The pass energy of the hemispherical analyser was maintained at 50 eV, giving a constant energy resolution of 0.53 eV. The uptake of oxygen on aluminium surfaces, at room temperature, was monitored by following the changes in the intensity of XPS Al 2p and O 1s photoelectron lines. A Shirley background subtraction was performed for all spectra as data preprocessing for the three-way PARAFAC.

RESULTS AND DISCUSSION

The real XPS data matrix (dimensions of $90 \times 15 \times 6$) for the three-way analysis is built up from all Al 2p spectra taken through studied ranges of exposure time and pressure. It consisted of six slices and on each slice there are 15 columns representing XPS spectra for 15 time levels at one pressure level. In three-dimensional space, the data matrix containing the XPS intensities is represented by three variables: the binding energy (BE) channel number (90 levels), the exposure time (15 levels) and the pressure (6 levels), all in increasing order. In the solution, factor loadings are extracted into three matrices: BE mode, time mode and pressure mode, corresponding to $\boldsymbol{A}$, and $\boldsymbol{B}$ and $\boldsymbol{C}$ matrices, respectively. The data and results of three-way analysis for the O 1s photoelectron lines will be presented in a separate publication.[25]

Figure 2 shows a representative slice set up from XPS Al 2p spectra collected at a water vapour pressure of 2.0×10^{-6} Pa. From Fig. 2 it can be seen that increasing exposure time causes a growth of oxide layers, resulting in an attenuation of the intensity of the Al 2p metallic component at BE 72.87 ± 0.05 eV and an increase of the Al 2p oxidic component at BE 75.80 ± 0.05 eV. Such evolutions of these components were observed for all other pressure levels and have been used as main features to verify the physical meaningfulness of the factor loadings in the time mode. The peak positions, in turn, were used to identify peaks in the BE mode.

The calculations were performed using the 'PMF3' program with all possible combinations of its options, i.e. weighted least-squares regression and non-negativity constraint, for 1–6 factors. Because the counts in the electron detection system obey Poisson statistics,[26] for weighted regression the standard deviation s_{ijk} of each element y_{ijk} in the data matrix is estimated from a simple formula: $s_{ijk} = n_1 + n_2(y_{ijk})^{1/2}$, where the adjustable coefficients n_1 and n_2 were chosen according to the signal-to-noise ratio in each spectrum; typically $n_1 = 0.1$ and $n_2 = 1.0$–1.5. In order to identify correctly the

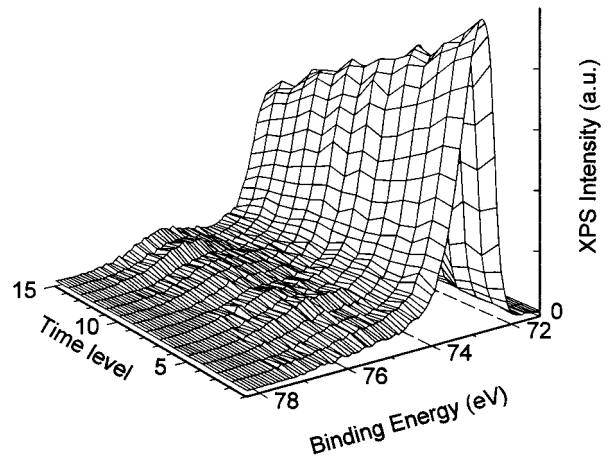

Figure 2. Representative slice (90 BE levels × 15 exposure levels) in the real XPS data matrix. All XPS Al 2p spectra were collected after exposing clean surfaces to water vapour at a pressure of 2.0×10^{-6} Pa.

global minimum solution, for each number of factors 20–50 different starting points of the iterative process were used. The solutions were then verified using the above experimentally observed features of components, the error residuals and the goodness of fit ($\chi^2 = Q/N$, where Q is the final sum of error squares, i.e. Eqn. (2) or Eqn. (3); and N is the number of elements in the data matrix, in our case $N = 90 \times 15 \times 6 = 8100$).

Figure 3 shows the goodness of fit vs. the number of factors from solutions obtained with four possible different options used: unweighted and unconstrained, unweighted and constrained, weighted and unconstrained and weighted and constrained. In all options the goodness of fit is better, i.e. the χ^2 value decreases as the number of factors increases, simply because the more components extracted the better the variation structure is fitted and the less residuals are left. However, beyond the true number of factors the data is

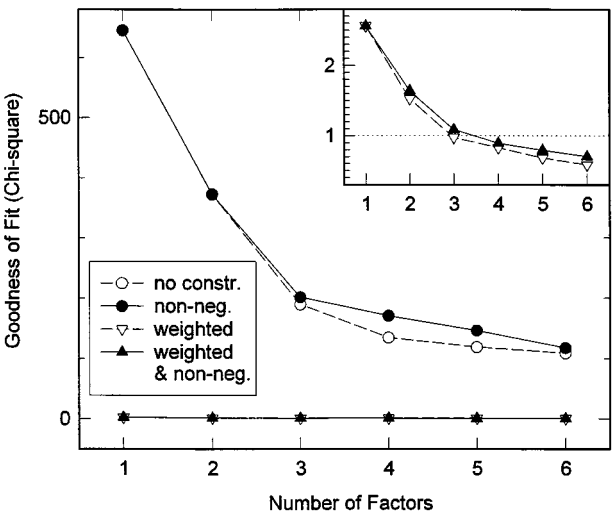

Figure 3. The goodness of fit (χ^2) vs. number of factors using four possible options of the 'PMF3' program: no weighted regression and no constraint on non-negativity (no constr.), no weighted regression but with constraint on non-negativity (non-neg.), weighted regression but no constraint (weighted) and with weighted regression and constraint on non-negativity (weighted & non-neg.).

modelled not only by more correlated components but also by fitting the noise structure; consequently, the fit will improve only by noticeably smaller amounts. A gradual change in the fit after the factor number reached three (shown in Fig. 3) suggests that the correct, true number of factors for modelling our data might be three. It should be noted that the χ^2 value obtained in solutions with three factors in ~ 1.0, which is the best value for fitting if the error modelling is correct.

Figure 4 shows the three-factor solution using only the weighted regression option in the 'PMF3' program. The negative values and, in particular, the distorted shapes of XPS spectra in the BE mode—also observed in all solutions only with weighted regression for the

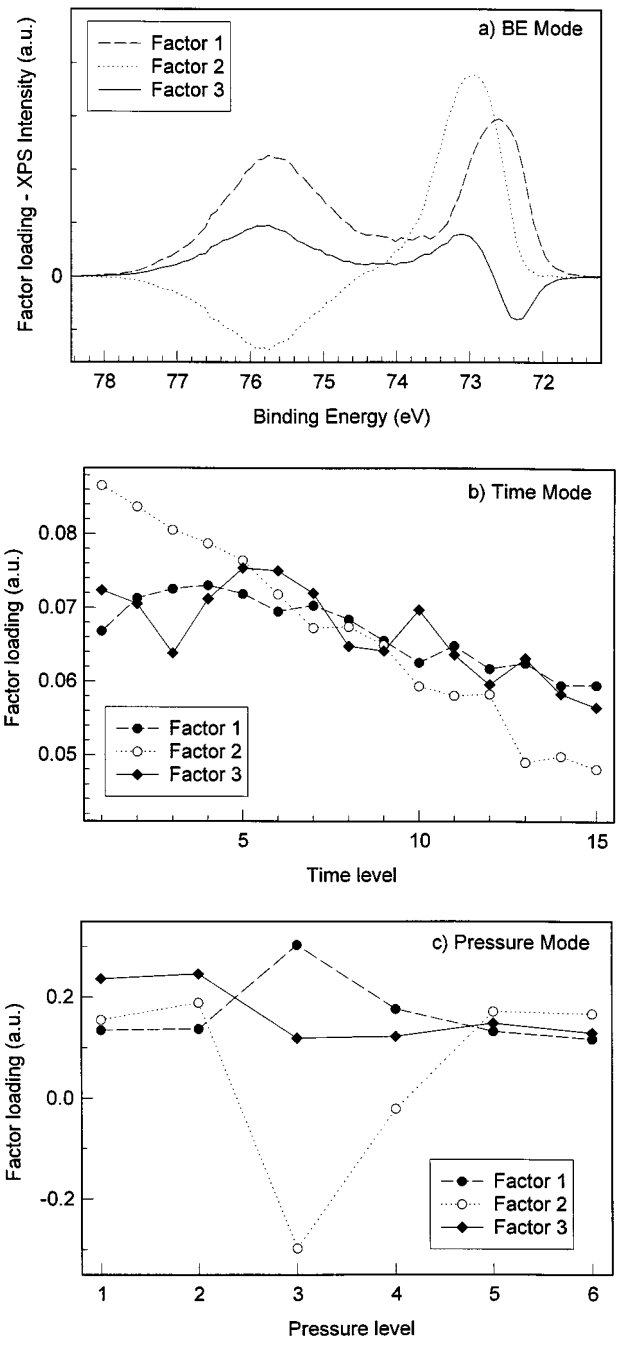

Figure 4. Factor loadings of the solution using the 'PMF3' program for the three-factor model with weighted regression only: (a) BE mode; (b) time mode; (c) pressure mode.

number of factors other than three (except for one factor; the case of a model with one factor will not be discussed further because of an apparent multiple-peak structure in the XPS spectrum)—are physically meaningless. The high correlation between factors, which appears often in the degeneracy problem of PARAFAC solution,[27] suggests that these factors are not clearly identifiable. Thus the PARAFAC model may not yield the same solution for different starting points of the iterative procedure in the space where negative factor loadings are allowed. For example, Fig. 5 represents two different solutions obtained from two different starting points (three factors, weighted regression only) having the same χ^2 value. Similar results were obtained in solutions without the weighted regression. Figure 6 shows the BE mode in a solution solved for the three-factor model without any constraints [Fig. 6(a)], unweighted and no non-negativity constraint) and with constraint on non-negativity only [Fig. 6(b)], unweighted and with non-negativity constraint). As observed above, the unweighted without non-negativity constraint solution is unacceptable because of negative values present; imposing the non-negativity constraint may properly extract the largest factor [factor 3 in Fig. 6(b); also compare with factor 4 in Fig. 7 and factor 1 in Fig. 8(a) discussed below], but the smaller factors cannot be totally distinguished. Instead, they are present in the remaining factors in different linear combinations, which also involve the largest factor in models with more than three factors. In consequence, both weighted regression and the non-negativity constraint should be applied when analysing the XPS data; all PARAFAC solutions presented hereafter will refer to those solved by the 'PMF3' program using all these options.

If too many factors are extracted, the largest factor may be similar regardless of factor number but the smallest factor(s) may be fitting errors and/or be combined partially with the variance structure from the largest factor and therefore may be unreliable. Thus, the PARAFAC solution may not be the same from different starting points. Figure 7 represents two selected differ-

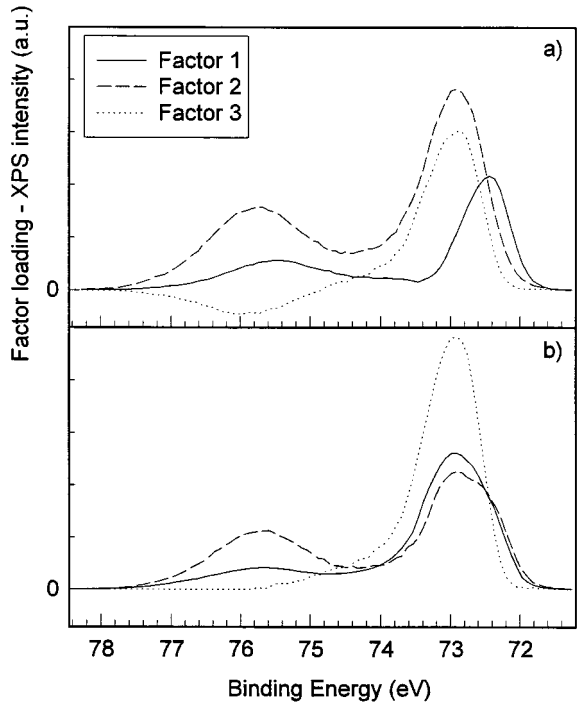

Figure 6. The BE mode in the solutions of the three-factor model: (a) no weighted regression and no constraint on non-negativity; (b) no weighted regression and with constraint on non-negativity only.

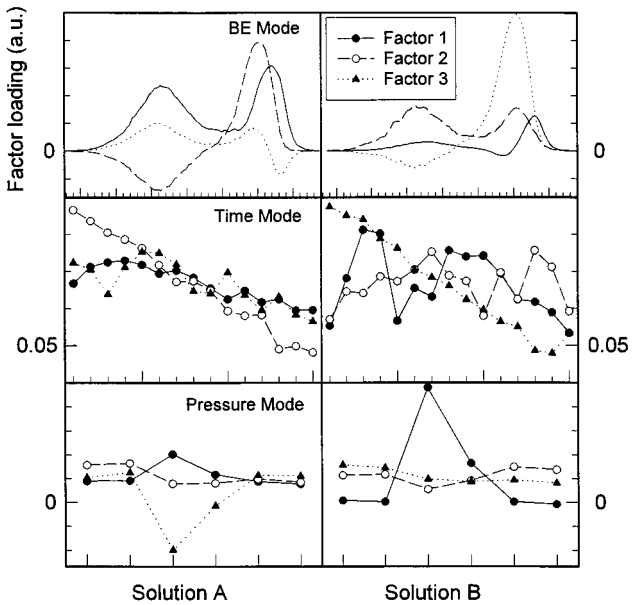

Figure 5. Three-factor model with weighted regression only: two different solutions having the same goodness of fit value (χ^2) obtained for two different starting points in the iterative process. For comparison, the scales of factor loadings in each mode are the same in both solutions *A* and *B*; the horizontal scales in BE, time and pressure mode are as shown in Fig. 4(a), 4(b) and 4(c), respectively.

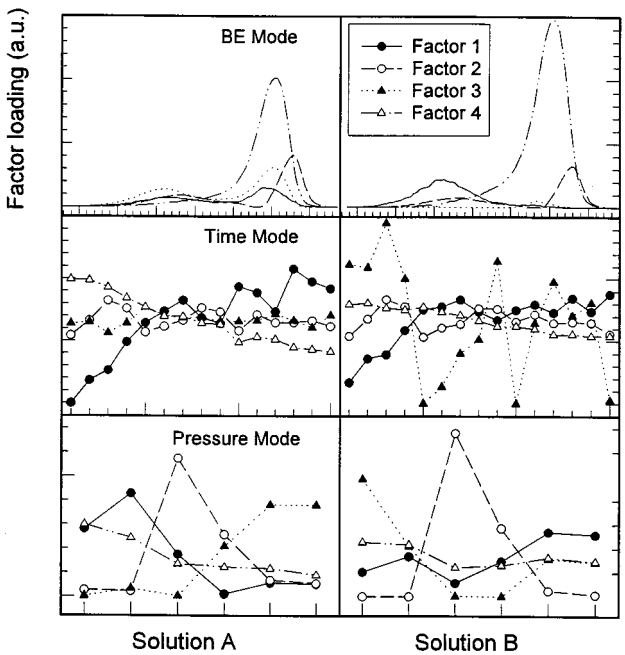

Figure 7. Four-factor model with weighted regression and constraint on non-negativity: two different solutions having the same goodness of fit value (χ^2) obtained for two different starting points in the iterative process. For comparison, the scales of factor loadings in each mode are the same in both solutions *A* and *B*; the horizontal scales in BE, time and pressure mode are as shown in Fig. 4(a), 4(b) and 4(c), respectively.

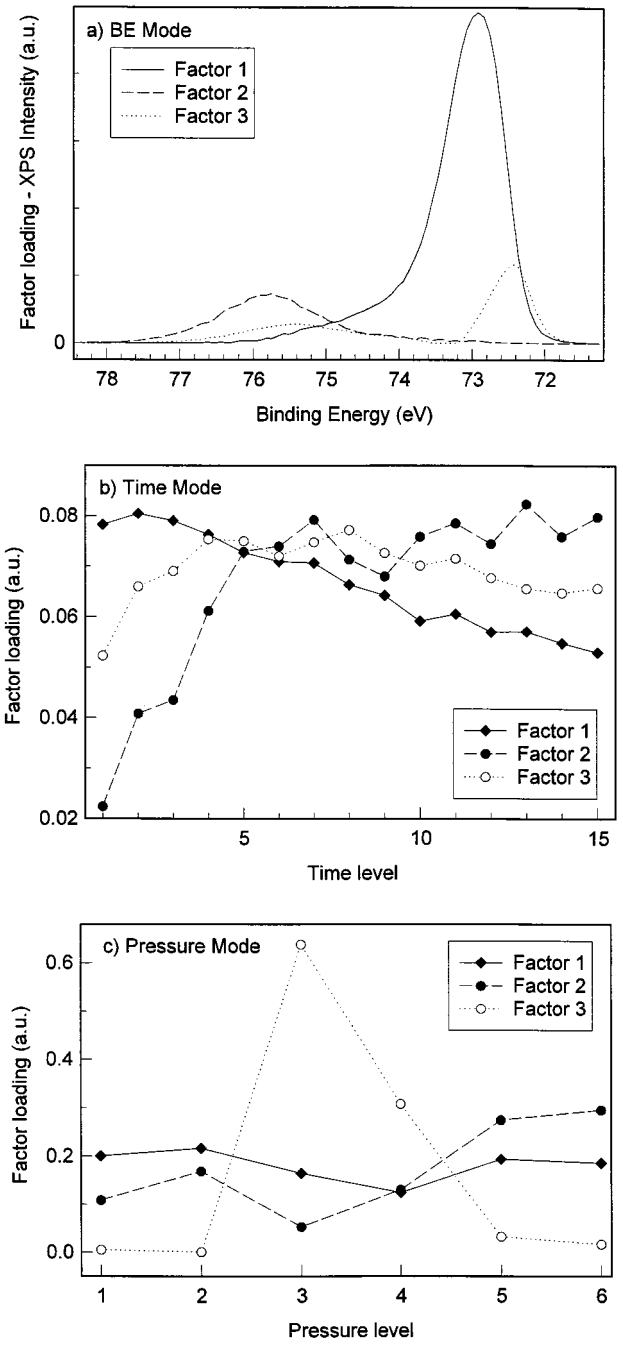

Figure 8. Factor loadings of the solution using the 'PMF3' program for the three-factor model with weighted regression and constraint on non-negativity: (a) BE mode; (b) time mode; (c) pressure mode.

ent solutions (found from two different random starting positions for a four-factor model) with the same final goodness of fit. It is evident that the largest factor, factor 4, behaves similarly for both solutions across all modes; the smaller factor, factor 2, also shows the same properties. By contrast, the remaining two factors (factors 1 and 3) have two different sets of loadings, showing in one solution where the noise is being increasingly modelled (see factor loadings in time mode, solution *B*) and in the other where the true factors are being modelled by correlated components (high correlations between factors can be seen across modes in solution *A*). These two effects also occur in solutions with more than four factors.

By contrast, the same solutions were obtained for all different randomly initiated starting points by PARAFAC for two and three factors. Figure 8 shows three modes in the solution of the three-factor model. As shown in Fig. 8, the largest factor, factor 1, in similar across all modes in four-factor solutions (see factor 4 in Fig. 7). Moreover, this factor is also maintained in the solution for two factors [see factor 2 in Fig. 9(a)]. The other factor in the two-factor solution seems to be a combination of two components, which when separated can become the solution for three factors shown in Fig. 8. Apparently, at this point the two-factor model, expect for the fact that it has higher χ^2 value (see Fig. 3), is as good as the three-factor model. Further examination of the fit of these two models is required to select the proper one for the final solution. This is discussed below.

Figure 9 presents a comparison between the experimental XPS Al 2p spectrum and the spectrum reconstructed using the two- and three-factor solutions. In this particular case, the experimental spectrum was collected after exposure of a clean aluminium surface to water vapour at a pressure of 1.3×10^{-5} Pa for 5 min. The reconstructed spectrum was calculated using Eqn. (7) for time level 5 and pressure level 3. The reduced χ^2 values of the fit of the normalization factors $v_2 = 80$ (two-factor model) and $v_3 = 76$ (three-factor model) calculated using the expression given by Cumpson and Seah [Eqn. (5) in Ref. 26] are 3.32 and 0.95, respectively. On their map of reduced χ^2 *vs.* v, the value of 0.95 for the three-factor model falls between the contours for $Q = 0.1587$ and $Q = 0.8413$ ($Q(\tau|v)$ is a probability distribution function for a good fit with $\chi^2 > \tau$; Eqn. (9) and Fig. 3 in Ref. 26). This value indicates that the region for fits is dominated by random differences between the model and the real spectrum and verifies that the fit of the three-factor model is acceptable. By constrast, the χ^2 value of 3.32 for the two-factor model is definitely too large for the differences to be random. Figure 10 also shows the error residuals after fitting with the two- and three-factor models calculated for six spectra on time level 15 (60 min of exposure) and for all six levels across the entire pressure range. From Fig. 10, the three-factor model has a better fit than that for the two-factor model; its χ^2 values range from 0.96 to 1.05, which are good values for a fit based on the reference of Cumpson and Seah.[26] The same spectra fitted with the two-factor model show different χ^2 values; two of them, 0.41 and 0.37 are too small, and the next two, 2.75 and 4.04, are too large, respectively, for a random different in residuals; only two values, 0.84 and 1.05, are acceptable. A similar examination of the rest of the spectra in the data matrix shows that over 60% of the spectra are improperly fitted using the two-factor model (χ^2 is either too small or too large). Consequently, the three-factor model can be postulated as the most suitable to use in the PARAFAC of our XPS data.

Interpretation of the PARAFAC solution

The three factors represented in the solution from Fig. 8 can be identified as follows.

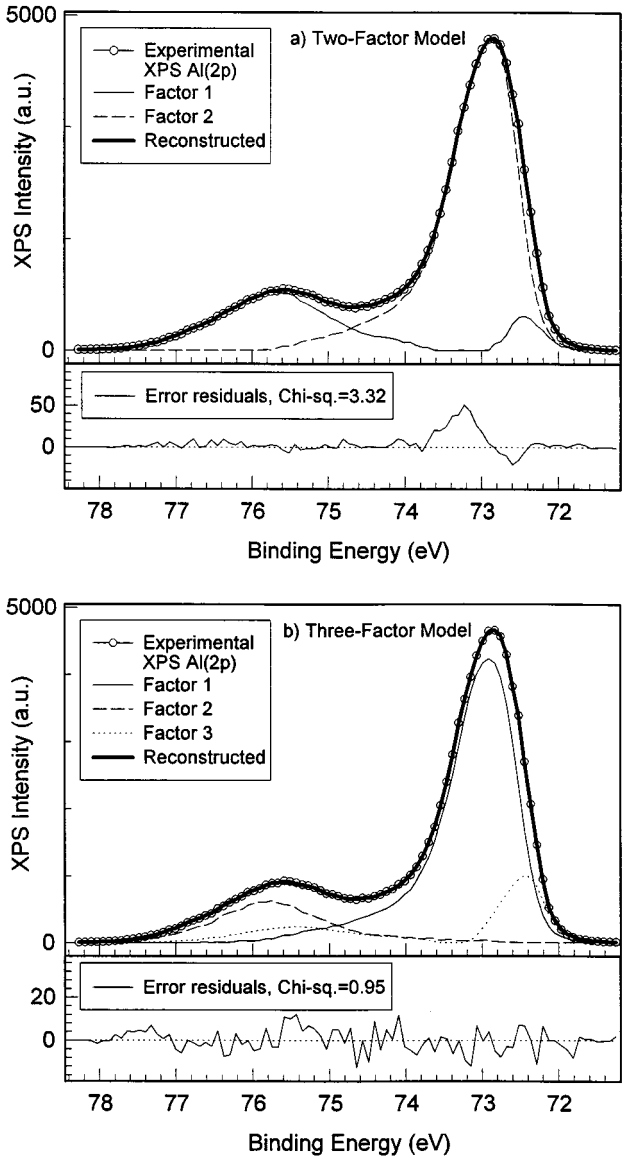

Figure 9. Comparison of an experimental XPS Al 2p spectrum with a reconstructed spectrum using the PARAFAC method for: (a) the two-factor model; (b) the three-factor model (more details in text). Top part shows the fit with factors; bottom part shows the error residuals after fitting and the calculated value of χ^2 (Chi-sq.)

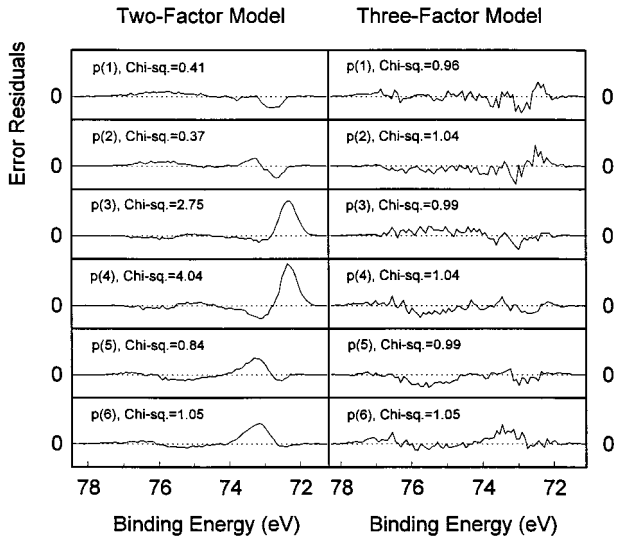

Figure 10. Error residuals obtained after fitting by the PARAFAC technique using the two-factor (left) and three-factor (right) model for all pressure levels and time level 15 (more details in text). For comparison, the scales of error residuals remain the same in all graphs.

Factor 1. Based on the peak position (BE-72.9 eV) and peak shape in the BE mode in Fig. 8(a), this factor can be identified as the pure metallic Al 2p peak. Verification that factor 1 represents an XPS Al 2p spectrum of aluminium with a clean surface can be provided by comparing its factor loadings in the BE mode with photoelectron intensities in the real spectrum. As shown in Fig. 11, the peak represented by the factor loadings (dashed line) exactly reproduces the XPS Al 2p spectrum (solid line) obtained for aluminium after surface cleaning by Ar^+ ion bombardment. Figure 8(b) shows the evolution of loadings of factor 1 through the time levels, which reflects the attenuation of the metallic peak due to a growth of thin oxide films with increasing exposure time. In the pressure mode [Fig. 8(c)], as expected, the factor 1 loadings remain practically unchanged across all pressure levels, indicating independence of the metallic peak from effects of water vapour pressure.

Factor 2. From Fig. 8(a), factor 2 is shown as a single peak located at a BE of 75.8 eV, which can be assigned to the oxidic component in the XPS Al 2p spectrum. Again, the evolution of this peak in the time mode [Fig. 8(b)] confirms its identification in the BE mode, showing an increase in factor loading with increasing exposure time and corresponding to the growth of oxide on the aluminium surface. In the pressure mode [Fig. 8(c)], factor 2 loadings show a slight increase with increasing pressure.

Factor 3. Figure 8(a) shows factor 3 as a double peak with maxima at 72.4(4) and 75.4(3) eV. These are new

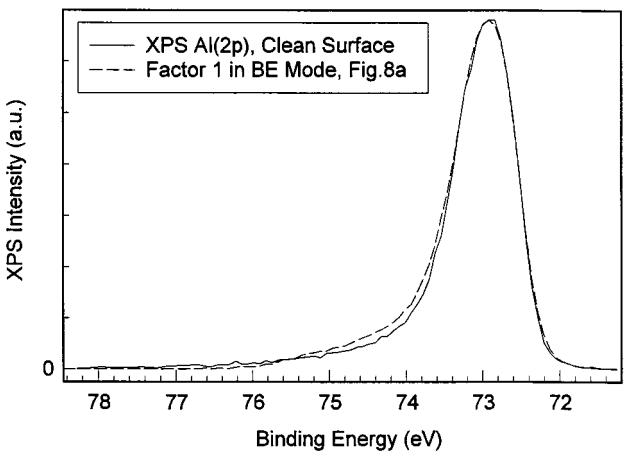

Figure 11. Comparison between factor 1 loadings from the BE mode [Fig. 8(a)] and the real intensities of the XPS Al 2p spectrum obtained for a clean surface. The peak heights are normalized to the same value.

components in the XPS Al 2p spectrum, the existence of which has only been assumed based on consideration of possible elemental processes in the oxidation of aluminium. In the time mode [Fig. 8(b)] the factor 3 loadings increase as the exposure time increases and then slightly decrease after 5 min of exposure. In the pressure mode [Fig. 8(c)] the factor loading has a maximum at pressure level 3 (1.3×10^{-5} Pa). The full identification of these components is discussed further below.

From the literature, the adsorption of water on clean aluminium surfaces at temperatures below 100 K is associative, i.e. mainly molecular;[28–30] upon heating to 125–150 K the adsorption is competitively associative and dissociative[31,32] and from $\sim$300 K upwards it is completely dissociative.[33] At room temperature, therefore, the adsorption of water molecules on clean aluminium surfaces results in three possible elementary adsorbed species: hydroxyl groups [OH(ad)], hydrogen [H(ad)] and oxygen [O(ad)] atoms. Further reaction leads to the formation of different chemical bonds with aluminium atoms, such as Al–O in oxides and hydroxides and Al–H in hydrides, which will be reflected in the number of peaks present in the XPS spectrum of aluminium and the peak position in binding energy.

It is well known that Al–O chemical bonding is dominated by ionic character, in which the aluminium atom tends to donate its valence electrons to the oxygen atom, resulting in reduction of the valence electron density and leading to an increase in the Al 2p core electron binding energy. The chemical shift of aluminium in thin oxide films is well documented in the paper of Olefjord *et al.*,[34] which is a summary of the tests from 20 laboratories worldwide to find a standard data set necessary for quantitative surface analysis of the Al_2O_3/Al system. These tests have established that in an XPS Al 2p spectrum the binding energy of the metallic state Al^0 and the chemical shift of Al^{3+} in the oxide layer are 73.0 ± 0.1 eV and 2.8 ± 0.1 eV (i.e. the oxide state Al^{3+} has a BE of 75.8 eV), respectively. Our experimentally observed values of binding energies for metallic and oxidic peaks (72.87 ± 0.05 and 75.80 ± 0.05 eV) and those extracted by PARAFAC (Fig. 8) (72.9 and 75.8 eV, respectively) are in good agreement with the above values.

The third factor extracted by PARAFAC, shown in Fig. 8(a), has a shape with distinct defined positions of maxima and their discrepancies, which clearly indicates a two-peak structure. These two peaks might represent the contributions from two other distinguished chemical bonds with aluminium to the XPS Al 2p spectrum. These two peaks in the third factor cannot be the result of a charge-broadening effect of the following reasons. Firstly, no charging effect was observed for the adventitious reference C 1s peak; this centroid was found at a BE of 286.20 ± 0.05 eV, which satisfactorily agrees with the value from the tests of Olefjord *et al.*,[34] i.e. 285.8 ± 0.3 eV. In addition, a value of 286.4 ± 0.3 eV is recommended for use as a charge reference for aluminium oxide (V. Crist, XPS International, Inc., http://www.xpsdata.com/ personal communication). Secondly, a systematic peak shift would increase as the oxide grows in thickness and would result in strong fluctuations in values of factor loadings in all modes.

Thus, the appearance of two peaks in one factor indicates that these two components (the formation of two chemical species) are associated in a chemical process. For the third factor, the peak at a binding energy of 75.4 eV, located between oxidic and metallic states at binding energies of 75.8 and 72.9 eV, respectively, can be identified intuitively as a contribution from other oxidized species, so the assignment of the associated peak at a BE of 72.8 eV needs additional discussion. The negative shift is binding energy of the XPS Al 2p peak observed at 72.4 eV would result from an increased density of states (DOS) in the valence band; typically, carbide, boride and hydride compounds have been found to cause this shift in some metals.[35] In the absence of other detectable elements, the formation of surface aluminium hydride is the only one that is possible. Using electron energy-loss spectroscopy (EELS), Paul and Hoffmann[36] reported the presence of an AlH_x species (x is likely to be 2) located at the metal/oxide interfaces during the interaction of Al(100) with water vapour. This interface hydride has been suggested in other systems using different techniques, such as Al(100)/H by EELS and thermal desorption spectroscopy (TDS),[37] Al(110)/O_2 by high-resolution EELS[38] and Al–Al_2O_3–Pb junctions by inelastic electron tunnelling spectra (IETS).[39,40] It has been found that the parabolic s-p bands of aluminium in AlH and AlH_2 are drastically modified by metal–hydrogen interaction. Based on comparison of the energy bands and DOS between pure Al and the hydrides AlH and AlH_2, Gupta and Burger[41] showed that both hydrides are metallic and both have a DOS at the Fermi level (E_F) that is $\sim$25% higher than in the pure metal. Therefore, an aluminium hydride formed during the interaction of aluminium surfaces with water could possibly contribute a peak in the XPS Al 2p spectrum with a BE lower than the metallic peak. Consequently, the peak at a BE of 72.4 eV in the third factor extracted by PARAFAC [Fig. 8(a)] may be assigned to an aluminium hydride.

Our PARAFAC solution also supports the assumption of hydride at the metal/oxide interface. Such a conclusion can be drawn on the basis of the variation of factor 3 loading in the time mode [see Fig. 8(b)]; as the exposure time increases, the factor loading increases up to $\sim$5 min and then undergoes a slight decrease. This suggests that Al–H bonds would be found at the metal/oxide interface; aluminium hydride could be formed on clean surfaces at the very initial stages, competitively with other species such as oxide and hydroxide. After oxide coalescence, due to the higher electron affinity of oxygen,[42] surface hydrogenation is limited or entirely stopped and the hydride species is covered by an oxide overlayer. This would explain the decreasing behaviour in the third factor loading in the time mode. Finally, it is interesting to note that the variation of loading of the oxide has a break at the same point where the loading of the hydride component reaches its maximum value. This may be important in view of the corrosion properties of thin aluminium oxide films, suggesting that the hydride at the metal/oxide interface possibly causes a reduction in oxidation rate.

Further, the association of two peaks in the third factor means that these two components may arise at the same time and develop in the same way through the entire range of time and pressure variables. If so, the PARAFAC model should not identify these two components as two separate factors. The peak association in

the third factor can be explained using the reaction

$$2(a+b)Al^0 + 2H_2O \rightarrow 2\ Al_aOH_y + 2\ Al_bH_x + [2-(x+y)]H_2\uparrow \quad (8)$$

where Al_aOH_y can represent intermediate aluminium–oxygen structures such as Al–O–H, Al=O or Al–O–Al; these are the possible oxidized species, other than Al_2O_3, that will contribute to the peak at lower binding energy, i.e. the peak in the third factor at 75.4 eV. From reaction (8) it is clear that the ratio between the number of aluminium atoms bonded to hydrogen and the number of other oxidized aluminium atoms bonded to oxygen in $\boldsymbol{b/a}$. Such a ratio might be represented by the ratio of peak areas between the hydride and the oxide peak in the third factor of the BE mode [Fig. 8(a)], which has been estimated as 1.6. However, there are several other processes that could effect this ratio, including hydrogen recombination or decomposition reaction of the hydride

$$H(ad) + H(ad) \rightarrow H_2(g)\uparrow \quad (9)$$

$$Al_bH_x \rightarrow b\ Al + \frac{x}{2}\ H_2(g)\uparrow \quad (10)$$

Intermediate oxidized aluminium species can also be converted, as follows

$$2AlO + O(ad) \rightarrow Al_2O_3 \quad (11)$$

$$2AlOH + O(ad) \rightarrow Al_2O_3 + H_2(g)\uparrow \quad (12)$$

$$AlO + OH(ad) \rightarrow AlOOH \quad (13)$$

$$AlOH + O(ad) \rightarrow AlOOH \quad (14)$$

In the pressure mode, the hydride factor loadings show a maximum at pressure level 3, i.e. at the pressure of 1.3×10^{-5} Pa. The increase at lower water pressure can be explained by the simple proportional relationship between the number of water molecules impinging on the aluminium surface and pressure; as the amount of H(ad) increases with the water vapour pressure, the formation of hydride increases accordingly. By contrast, at pressures higher than 1.3×10^{-5} Pa the formation of an aluminium hydride drastically decreases, as indicated by the factor loadings at pressure levels 4, 5 and 6. This suggests that a significant change in reaction (8) or in one of its related processes [reactions (9)–(14)] has occurred during transition of the pressure to higher level. From reaction (8), it is apparent that reduction of an aluminium hydride can result only from an increase in the rate of any of the reactions (9)–(14). As was established previously, the stretching vibration at 1910 cm^{-1} in the EELS spectrum survived even flashes to 650 K,[43] providing the stability of the Al–H bonding; therefore a decomposition reaction of AlH_x may be neglected or may not occur at all in our experimental conditions. Then, the observed decrease of hydride can be attributed only to an increase in the desorption of hydrogen atoms in the recombination reaction (9), which results in turn in a rate increase in reactions (11)–(14) in order to keep the $\boldsymbol{b/a}$ ratio in reaction (8) constant. This may possibly be due to a change in the mechanism of hydrogen desorption from the aluminium surface in the range of pressure studied. This is discussed below.

Desorption of hydrogen from H-adsorbed aluminium surfaces at low H coverage has been found to obey zero-order or near-zero-order desorption kinetics.[43,44] This is a coverage-independent associative desorption, where hydrogen desorbs preferentially from active centres such as step or kink sites on aluminium surfaces after hydrogen diffusion from the rest of the surface. The activation energy for diffusion parallel to the surface is sufficiently small (0.1–0.2 eV[45]) to support this assumption. Because the density of active centres on aluminium surfaces is constant, the desorption rate of hydrogen is then relatively stable and therefore has no effect on the formation of hydride during variation of the pressure $< 1.3 \times 10^{-5}$ Pa. On the other hand, the saturation coverage of hydrogen adsorbed on aluminium surfaces has been found to vary from one monolayer (ML) for Al(111) (1.41×10^{15} atoms cm^{-2}) to 2.4 ML for Al(110) (2.07×10^{15} atoms cm^{-2}), respectively.[46] According to the TDS results of Winkler *et al.*,[46] the saturation coverage for hydrogen decreases approximately by an order of magnitude as the oxygen precoverage increases up to 0.11 ML (9.46×10^{13} atoms cm^{-2}). Moreover, these results show also that the presence of oxygen on the surface alters the conditions needed for zero-order and changes it to second-order desorption kinetics, which was apparently seen already from the 0.02 ML (2.06×10^{13} atoms cm^{-2}) oxygen precoverage. Now, assuming a water sticking coefficient of unity and complete de-hydrogenation, one may estimate that the desorption of hydrogen may change the kinetics order at water vapour pressures higher than 5.73×10^{-6} Pa and the surface saturation of hydrogen may occur at a water vapour pressure of 1.96×10^{-5} Pa for Al(111) or 2.88×10^{-5} Pa for Al(110). At a water vapour pressure of 1.3×10^{-5} Pa, where the maximum factor loading for the hydride is observed, adsorption of hydrogen on aluminium surfaces may have reached the saturation level and the desorption may have switched to second order, which yields a rate proportional to the square of hydrogen coverage. Consequently, as the pressure of water vapour increases beyond 1.3×10^{-5} Pa, the rate of formation of hydride decreases rapidly, explaining its variation in factor loading in the pressure mode. In order to maintain the $\boldsymbol{b/a}$ ratio in reaction (8) constant, an increase in the factor loading of the oxidic peak in the pressure mode would occur. From Fig. 8(c) it is evident that a slight increase in factor loading occurs for the oxidic component at pressures higher than 1.3×10^{-5} Pa.

CONCLUSION

We have shown the use of the three-way PARAFAC model to decompose a set of XPS Al 2p spectra obtained in the study of oxidation of aluminium by water vapour. The three variables used were: time of exposure, pressure of exposure and XPS binding energy. The PARAFAC method is shown to be a useful tool in XPS analysis, with its capacity to dissect a complex system into a set of independent components that are interpretable using basic physical parameters.

A weighted least-squares algorithm with non-negativity constraint is most suitable for the three-way PARAFAC of XPS data. These constraints were important because they removed what otherwise would have been an ambiguity due to partial non-independence of

factor variations. Three factors were extracted from the XPS Al 2p data: the metallic peak at BE 72.9 eV, the oxidic peak at BE 75.8 eV and a new third component with two peaks at BE 72.4 and 75.4 eV, respectively.

The third component in the XPS Al 2p spectrum has been fully identified with the peak at a BE of 72.4 eV for an aluminium hydride and the associated peak for other oxidized aluminium at a BE of 75.4 eV. Evolution of the third peak as a function of exposure time suggests that the aluminium hydride was formed at the metal/oxide interface. Moreover, evolution of the third peak during the variation of pressure shows a reduction of the aluminium hydride at a pressure of $>1.3 \times 10^{-5}$ Pa, presumably due to an increase of recombination of atomic hydrogen.

Acknowledgement

The authors wish to thank Dr P. Paatero for kind permission to use the 'PMF3' program and helpful discussions, and Alcan for supplying the aluminium samples used in this study.

REFERENCES

1. M. P. Seah, in *Practical Surface Analysis*, ed. by D. Briggs and M. P. Seah, 2nd Edn, Vol. 1, p. 201. Wiley, Chichester (1990).
2. G. Faraci, S. La Rosa, A. R. Pennisi, Y. Hwu and G. Margaritondo, *Phys. Rev. B* **47**, 4052 (1993); *J. Appl. Phys.* **78**, 4091 (1995).
3. C. F. McConville, D. L. Seymour, D. P. Woodruff and S. Bao, *Surf. Sci.* **188**, 1 (1987).
4. C. Berg, S. Raaen, A. Borg, J. N. Andersen, E. Lundgren and R. Nyholm, *Phys. Rev. B* **47**, 13063 (1993).
5. C. Palacio and H. J. Mathieu, *Surf. Interface Anal.* **16**, 178 (1990).
6. J. N. Fiedor, A. Proctor, M. Houalla and D. M. Hercules, *Surf. Interface Anal.* **20**, 1 (1993).
7. S. J. Scierka, A. Proctor, M. Huoalla, J. N. Fiedor and D. M. Hercules, *Surf. Interface Anal.* **20**, 901 (1993).
8. R. A. Harshman, *UCLA Working Pap. Phonet.* **16**, 1 (1970).
9. J. D. Carroll and J. Chang, *Psychometrika* **35**, 283 (1970).
10. D. S. Burdick, X. M. Tu, L. B. McGown and D. W. Millican, *J. Chemom.* **4**, 15 (1990).
11. J. K. Lee, R. T. Ross, S. Thampi and S. Leurgans, *J. Phys. Chem.* **96**, 9158 (1992).
12. S. Leurgans and R. T. Ross, *Stat. Sci.* **7**, 289 (1992).
13. E. Sanchez and B. R. Kowalski, *J. Chemom.* **4**, 24 (1990).
14. R. A. Harshman, UCLA *Working Pap. Phonet.* **22**, 111 (1972).
15. J. B. Krukal, *Psychometrika*, **41**, 281 (1976); *Linear Algebra Appl.* **18**, 95 (1977).
16. J. Deleeuw and S. Pruzansky, *Psychometrika* **43**, 83 (1978).
17. R. A. Harshman and M. E. Lundy, *Comput. Stat. Data Anal.* **18**, 39 (1994).
18. S. Leurgans, R. T. Ross and R. B. Abel, *SIAM J. Matrix Anal. Appl.* **14**, 1064 (1993).
19. C. L. Lawson and R. J. Hanson, *Solving Least Squares Problems*, Chapt. 23. Prentice-Hall, Englewood Cliffs, NJ (1974).
20. P. J. Gemperline, *Anal. Chem.* **58**, 2656 (1986).
21. R. T, Ross and S. Leurgans, *Methods Enzymol.* **246**, 679 (1995).
22. P. Paatero, *Chem. Intell. Lab. Syst.* **38**, 223 (1997).
23. P. Paatero and U. Tapper, *Environmetrics* **5**, 111 (1994).
24. C. J. Powell, in *Quantitative Surface Analysis of Materials*, ed. by N. S. McIntyre, ASTM Publication 643, p. 5. ASTM, Philadelphia, PA, (1978).
25. T. Do and N. S. McIntyre, *Surf. Interface Anal.*, Submitted for publication (1999).
26. P. J. Cumpson and M. P. Seah, *Surf. Interface Anal.* **18**, 345 (1992).
27. J. B. Kruskal, R. A. Harshman and M. E. Lundy, in *Multiway Data Analysis*, ed. by R. Coppi and S. Bolasco, p. 115. North-Holland, New York, (1989).
28. U. Memmert, S. J. Bushby and P. R. Norton, *Surf. Sci.* **219**, 327 (1989).
29. S. J. Bushby, B. W. Callen, K. Griffiths, F. J. Esposto, R. S. Timsit and P. R. Norton, *Surf. Sci. Lett.*, **298**, L181 (1993).
30. J. C. Fuggle, L. M. Watson, D. J. Fabian and S. Affrossman, *Surf. Sci.* **49**, 61 (1975).
31. F. P. Netzer and T. E. Madey, *Surf. Sci.* **127**, L102 (1983).
32. F. J. Szalkowski, *J. Chem. Phys.* **77**, 5224 (1982).
33. J. E. Crowell, J. G. Chen, D. M. Hercules and J. T. Yates, Jr., *J. Chem. Phys.* **86**, 5804 (1987).
34. I. Olefjord, H. J. Mathieu and P. Marcus, *Surf. Interface Anal.* **15**, 681 (1990).
35. J. F. Moulder, W. F. Stickle, P. E. Sobol and K. D. Bomben, in *Handbook of X-ray Photoelectron Spectroscopy*, ed. by J. Chastain, Perkin-Elmer, Eden Prairie, MN (1992).
36. J. Paul and F. M. Hoffmann, *J. Phys. Chem.* **90**, 5321 (1986).
37. J. Paul, *Phys. Rev. B*, **37**, 6164 (1988).
38. P. A. Thiry, J. J. Pireaux, M. Liehr and R. Caudano, *J. Vac. Sci. Technol. A* **3**, 1439 (1985).
39. S. Gauthier, S. de Cheveigné, J. Klein and M. Belin, *Phys. Rev. B* **29**, 1748 (1984).
40. J. Igalson and J. G. Adler, *Phys. Rev. B* **28**, 4970 (1983).
41. M. Gupta and J. P. Burger, *J. Phys* **41**, 1009 (1980).
42. J. A. Dean, *Lange's Handbook of Chemistry*. McGraw-Hill, New York (1992).
43. J. M. Mundenar, R. Murphy, K. D. Tsuei and E. W. Plummer, *Chem. Phys. Lett.* **143**, 593 (1988).
44. A. Winkler, Ch. Resch and K. D. Rendulic, *J. Chem. Phys.* **95**, 7682 (1991).
45. H. Hjelmberg, *Surf. Sci.* **81**, 539 (1979).
46. A. Winkler, G. Požgainer and K. D. Rendulic, *Surf. Sci.* **251**/**252**, 886 (1991).